SCIENCE CHINA
Physics, Mechanics & Astronomy

• Review •
Special Topic: Quantum Information

July 2014 Vol. 57 No. 7: 1210–1217
doi: 10.1007/s11433-013-5358-0

Preparation of multipartite entangled states used for quantum information networks

SU XiaoLong, JIA XiaoJun, XIE ChangDe & PENG KunChi*

State Key Laboratory of Quantum Optics and Quantum Optics Devices, Institute of Opto-Electronics, Shanxi University, Taiyuan 030006, China

Received August 30, 2013; accepted September 27, 2013; published online March 6, 2014

The preparation of multipartite entangled states is the prerequisite for exploring quantum information networks and quantum computation. In this paper, we review the experimental progress in the preparation of cluster states and multi-color entangled states with continuous variables. The preparation of lager scale multipartite entangled state provide valuable quantum resources to implement more complex quantum informational tasks.

quantum information with optical qumodes, quantum computation, entangled state, continuous quantum variable

PACS number(s): 03.67.Bg, 03.67.Lx, 03.65.Ud, 42.50.Dv

Citation: Su X L, Jia X J, Xie C D, et al. Preparation of multipartite entangled states used for quantum information networks. Sci China-Phys Mech Astron, 2014, 57: 1210–1217, doi: 10.1007/s11433-013-5358-0

Developing quantum information (QI) science has exhibited unusual potentiality to realize qualitatively information processing with new modes which are unavailable in the classical world [1–3]. Optical QI based on exploiting discrete-variable (DV) of single-photon states (qubits) and continuous-variable (CV) of optical modes (qumodes) has an important role in the development of QI. So far, a variety of fundamental protocols for QI processing have been experimentally demonstrated [4–11]. To build practical QI systems applied in the real world we must establish QI networks, and thus the study on the preparation of multipartite and multi-color entangled states, which are the necessary resources for QI networks, becomes the crucially preceding task. The measurement-based one-way quantum computation (QC) utilizing multipartite cluster states provides a promising QI scheme, which has been extensively investigated in both DV and CV regimes [8–20]. Recently, the optical cluster states of eight-photon [21,22], eight-qumode [23, 24] and up to 10000-qumodes [25] have been successfully produced. On the other hand, to develop a complete quantum network composed of many nodes and channels, quantum memories usually constructed by atomic systems must be required [26–30]. The quantum connectivity in information networks, such as distributing entanglement throughout a network with large size and teleporting quantum states between nodes, can be accomplished by the interaction of light and atoms in quantum memories. Thus, it is necessary to prepare multi-color entangled states involving different wavelengths at atomic transitions for storing information and transparency windows of channels for transmitting quantum states with possibly low loss.

In this review article, we briefly introduce the physical conception of multipartite optical CV cluster states and different preparation methods. Then, we describe the graph and mathematic representations of CV eight-partite linear and two-diamond shape cluster states, deduce the inseparability criterion inequalities for quantitating the CV entanglement, and present the experimental set-up and results completed by our group. Successively, we discuss the research progress in the generation of CV multi-color entangled states in sect. 2. The generations of two-color entanglement are summarized and the three-color CV entanglement for qumodes are ana-

*Corresponding author (email: kcpeng@sxu.edu.cn)

lyzed, in which the theoretical protocol and the experimental demonstration achieved by our group are mainly introduced.

1 Optical cluster state with continuous variables

1.1 Basic conception

Cluster state is a type of multipartite quantum entangled graph states corresponding to some mathematic graphs [13–16]. The CV cluster quadrature correlations (so-called nullifiers) can be expressed by [14–16]

$$\left(\hat{p}_a - \sum_{b\in N_a} \hat{x}_b\right) \to 0, \quad \forall a \in G, \tag{1}$$

where $\hat{x}_a = (\hat{a} + \hat{a}^\dagger)/2$ and $\hat{p}_a = (\hat{a} - \hat{a}^\dagger)/2\mathrm{i}$ represent the quadrature-amplitude and quadrature-phase operators of an optical mode $\hat{a}$, respectively. The subscript a (b) expresses the designated mode $\hat{a}$ ($\hat{b}$). The modes of $a \in G$ denote the vertices of the graph G, while the modes of $b \in N_a$ are the nearest neighbors of mode $\hat{a}$. For an ideal cluster state the left-hand side of eq. (1) tends to zero, which represents a simultaneous zero eigenstate of the quadrature combination [16]. The CV cluster quantum entanglements generated by experiments are deterministic, but also are imperfect, the entanglement features of which have to be verified and quantified by the sufficient conditions for the fully inseparability of multipartite CV entanglement [31–34]. Different correlation combinations are given (left-hand side of eq. (1)) in a variety of CV cluster multipartite entangled states, which reflect the complexity and rich usability of these quantum systems. The expressions of the nullifiers for different graph states depend on the graph configuration.

1.2 Preparation methods

There are several different methods of preparing multipartite CV cluster states. The linearly optical transformation of squeezed states on a specially designed beam-splitter network is the initially and frequently used method [23,31–33]. In this way, the prepared cluster state is space-separated, which can be easily utilized to implement one-way QC. The drawback of this method is that with increasing of the entangled modes the complexity of the experimental setup is also subsequently increased. Using this method, space-separated four-mode and eight-mode CV cluster states are prepared experimentally in two labs, respectively [23,31–33].

Successively, the technique of the optical frequency comb is applied in the preparation of CV cluster states, with which the lager scale cluster states can be prepared in principle [34]. However, in this way, these entangled modes are not easily separated and thus the schemes of utilizing them to implement quantum information need to be redesigned.

Recently a new method of using spatial entanglement to prepare multipartite entangled state has been presented, in which a virtual beam-splitter network was applied and a eight-mode Greenberger-Horne-Zeilinger (GHZ) entangled state was obtained [35]. The advantage of this method is that the experimental setup is simpler than the initial scheme of optical transformation. The challenge in this technique is the manufacture of the necessary multi-pixel detector. When the number of entangled states increases the technic difficulty also increases correspondingly. Moreover the application of it is also not convenient since every entangled modes are detected simultaneously, and thus how to implement one-way QC based on the feedforward of the measured results on an individual mode needs to be reconsidered.

Currently a super large cluster state in the time domain with up to 10000 submodes has been experimentally produced by the technique of time-domain multiplexing [25]. When applying such a cluster state to implement QC, very fast feedforward loops are required.

1.3 Preparation of eight-partite CV cluster states

Figures 1(a) and (b) show the graph representations of CV eight-partite linear (a) and two-diamond (b) shape CV cluster states, respectively, each node of which corresponds to an optical mode and the connection lines between neighboring nodes stand for the interaction between the connected two nodes. From eq. (1) and Figure 1, we can write the nullifiers of the linear and the two-diamond shape CV cluster states, respectively, which are $\hat{p}_{L1} - \hat{x}_{L2} = \delta_{L1}$, $\hat{p}_{L2} - \hat{x}_{L1} - \hat{x}_{L3} = \delta_{L2}$, $\hat{p}_{L3} - \hat{x}_{L2} - \hat{x}_{L4} = \delta_{L3}$, $\hat{p}_{L4} - \hat{x}_{L3} - \hat{x}_{L5} = \delta_{L4}$, $\hat{p}_{L5} - \hat{x}_{L4} - \hat{x}_{L6} = \delta_{L5}$, $\hat{p}_{L6} - \hat{x}_{L5} - \hat{x}_{L7} = \delta_{L6}$, $\hat{p}_{L7} - \hat{x}_{L6} - \hat{x}_{L8} = \delta_{L7}$, $\hat{p}_{L8} - \hat{x}_{L7} = \delta_{L8}$ for the linear states; and $\hat{p}_{D1} - \hat{x}_{D3} - \hat{x}_{D4} = \delta_{D1}$, $\hat{p}_{D2} - \hat{x}_{D3} - \hat{x}_{D4} = \delta_{D2}$, $\hat{p}_{D3} - \hat{x}_{D1} - \hat{x}_{D2} = \delta_{D3}$, $\hat{p}_{D4} - \hat{x}_{D1} - \hat{x}_{D2} - \hat{x}_{D5} = \delta_{D4}$, $\hat{p}_{D5} - \hat{x}_{D4} - \hat{x}_{D7} - \hat{x}_{D8} = \delta_{D5}$, $\hat{p}_{D6} - \hat{x}_{D7} - \hat{x}_{D8} = \delta_{D6}$, $\hat{p}_{D7} - \hat{x}_{D5} - \hat{x}_{D6} = \delta_{D7}$, $\hat{p}_{D8} - \hat{x}_{D5} - \hat{x}_{D6} = \delta_{D8}$ for the two-diamond states, where the subscripts Li and Di ($i = 1, 2, \ldots, 8$) denote the individual nodes of the linear and the two-diamond shape cluster states, respectively, δ_{Li} and δ_{Di} express the excess noises resulting from the imperfect quantum correlations. When the variance of δ_{Li} (δ_{Di}) is smaller than the corresponding quantum noise limit (QNL) determined by vacuum noises, the correlations among the combined optical modes is within the quantum region, otherwise the quantum correlations do not exist.

The schemes of generating CV multipartite entangled states commonly used in experiments are to achieve a linearly optical transformation of input squeezed states on a specific beam-splitter network [15]. Assuming $\hat{a}_l$ and U_{kl} represent the input squeezed states and the unitary matrix of a given beam-splitter network, respectively, the output optical modes after the transformation are given by $\hat{b}_k = \sum_l U_{kl}\hat{a}_l$, where the subscripts l and k express the designated input and output modes, respectively. In our experiment, four quadrature-amplitude $\hat{x}$-squeezed states, $\hat{a}_m = \mathrm{e}^{-r}\hat{x}_m^{(0)} + \mathrm{i}\mathrm{e}^{+r}\hat{p}_m^{(0)}$ ($m = 1, 3, 5, 7$), and four quadrature-phase $\hat{p}$-squeezed states, $\hat{a}_n = \mathrm{e}^{+r}\hat{x}_n^{(0)} + \mathrm{i}\mathrm{e}^{-r}\hat{p}_n^{(0)}$ ($n = 2, 4, 6, 8$), are applied, where $\hat{x}_j^{(0)}$

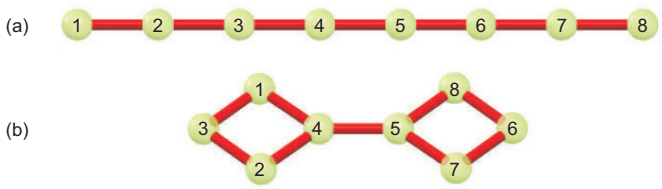

Figure 1 (Color online) Graph representation of eight-partite cluster states. (a) Linear cluster state [23]; (b) two-diamond shape cluster state. Each cluster node corresponds to an optical mode. The connected lines between neighboring nodes stand for the interaction among these nodes [24].

and $\hat{p}_j^{(0)}$ denote the quadrature-amplitude and the quadrature-phase operators of the corresponding vacuum field, respectively, r is the squeezing parameter to quantify the squeezing level, $r = 0$ and $r = +\infty$ correspond to the two cases of no squeezing and the ideally perfect squeezing,respectively. The unitary matrix for generating the CV eight-partite linear cluster state by combining eight squeezed states on optical beam splitters equals to

$$U_L = \begin{pmatrix} \frac{\mathrm{i}}{\sqrt{2}} & \frac{\mathrm{i}}{\sqrt{3}} & \frac{\mathrm{i}}{\sqrt{10}} & \frac{\sqrt{3}}{\sqrt{170}} & \frac{\sqrt{5}}{\sqrt{102}} & 0 & 0 & 0 \\ \frac{-1}{\sqrt{2}} & \frac{1}{\sqrt{3}} & \frac{1}{\sqrt{10}} & \frac{-\mathrm{i}\sqrt{3}}{\sqrt{170}} & \frac{-\mathrm{i}\sqrt{5}}{\sqrt{102}} & 0 & 0 & 0 \\ 0 & \frac{\mathrm{i}}{\sqrt{3}} & \frac{-\mathrm{i}\sqrt{2}}{\sqrt{5}} & \frac{-\sqrt{6}}{\sqrt{85}} & \frac{-\sqrt{10}}{\sqrt{51}} & 0 & 0 & 0 \\ 0 & 0 & \frac{\sqrt{2}}{\sqrt{5}} & \frac{3\mathrm{i}\sqrt{3}}{\sqrt{170}} & \frac{\mathrm{i}\sqrt{15}}{\sqrt{34}} & 0 & 0 & 0 \\ 0 & 0 & 0 & \frac{\sqrt{15}}{\sqrt{34}} & \frac{-3\sqrt{3}}{\sqrt{170}} & \frac{\mathrm{i}\sqrt{2}}{\sqrt{5}} & 0 & 0 \\ 0 & 0 & 0 & \frac{\mathrm{i}\sqrt{10}}{\sqrt{51}} & \frac{-\mathrm{i}\sqrt{6}}{\sqrt{85}} & \frac{\sqrt{2}}{\sqrt{5}} & \frac{1}{\sqrt{3}} & 0 \\ 0 & 0 & 0 & \frac{-\sqrt{5}}{\sqrt{102}} & \frac{\sqrt{3}}{\sqrt{170}} & \frac{\mathrm{i}}{\sqrt{10}} & \frac{-\mathrm{i}}{\sqrt{3}} & \frac{-\mathrm{i}}{\sqrt{2}} \\ 0 & 0 & 0 & \frac{-\mathrm{i}\sqrt{5}}{\sqrt{102}} & \frac{\mathrm{i}\sqrt{3}}{\sqrt{170}} & \frac{-1}{\sqrt{10}} & \frac{1}{\sqrt{3}} & \frac{-1}{\sqrt{2}} \end{pmatrix}. \quad (2)$$

The unitary matrix in eq. (2) expresses an optical transformation on a beam-splitter network consisting of seven beam splitters and can be decomposed into $U_L = F_8 I_7(-1) F_6^\dagger F_4 I_3(-1) F_2^\dagger B_{78}^-(1/2) F_8 B_{12}^-(1/2) F_1 B_{67}^-(1/3) F_7 B_{23}^-(1/3) F_2 B_{56}^-(2/5) F_6 B_{34}^-(2/5) F_3 B_{45}^+(25/34)$, where F_k denotes the Fourier transformation of mode k, which corresponds to a 90° rotation in the phase space; $B_{kl}^{\pm}(T_j)$ stands for the linearly optical transformation on the jth beam-splitter with the transmission of T_j ($j = 1, 2, \ldots, 7$), where $(B_{kl}^{\pm})_{kk} = \sqrt{1-T}$, $(B_{kl}^{\pm})_{kl} = \sqrt{T}$, $(B_{kl}^{\pm})_{lk} = \pm\sqrt{T}$, and $(B_{kl}^{\pm})_{ll} = \mp\sqrt{1-T}$, are elements of beam-splitter matrix. $I_k(-1) = \mathrm{e}^{\mathrm{i}\pi}$ corresponds to a 180° rotation of mode k in the phase space.

Figure 2 shows the schematic of the experimental set-up for preparing the eight-partite CV linear cluster state. The four $\hat{x}$-squeezed and four $\hat{p}$-squeezed states are produced by four NOPAs pumped by a common laser source, which is a CW intracavity frequency-doubled and frequency-stabilized Nd:YAP/LBO (Nd-doped $YAlO_3$ perorskite/lithium triborate) with both outputs of the fundamental and the second-harmonic waves [36]. The output fundamental wave at 1080 nm wavelength is used for the injected signals of NOPAs and the local oscillators of the balanced homodyne detectors (BHDs), which are applied to measure the quantum fluctuations of the quadrature-amplitude and the quadrature-phase of the output optical modes [31]. The second-harmonic wave at 540 nm wavelength serves as the pump field of the four NOPAs, in which through an intracavity frequency-down-conversion process a pair of signal and idler modes with the identical frequency at 1080 nm and the orthogonal polarizations are generated [7,37]. Each of NOPAs consists of an α-cut type-II KTP crystal and a concave mirror [37]. Since the amplitude and the phase quadratures of the signal and the idler modes are entangled each other, the two coupled modes of them at ±45° polarization directions both are the squeezed states [31,38]. In our experiment, the four NOPAs are operated at the parametric deamplification situation, that is the phase difference between the pump field and the injected signal is $(2n+1)\pi$ (n is an integer). Under this condition, the coupled modes at +45° and −45°polarization directions are the quadrature-amplitude and the quadrature-phase squeezed states, respectively [31,38]. When the transmissions of the seven beam splitters are chosen as $T1 = 25/34$, $T2 = T3 = 2/5$, $T4 = T5 = 1/3$, $T6 = T7 = 1/2$, the eight output optical modes $\hat{b}_j$ ($j = 1, 2, \ldots, 8$) are in a eight-partite CV linear cluster state. The quadrature-amplitude and quadrature-phase of each $\hat{b}_j$ are measured by eight BHDs, respectively. The nullifiers of the eight output modes depend on the squeezing parameters of the resource squeezed states. For our experimental system all four NOPAs have the identical configuration and are operated under identical conditions. Each of NOPAs is also adjusted to produce two balanced squeezed states. Thus, the eight initial squeezed states own the same squeezed parameter r. In this case we can easily calculate the excess noises of the nullifiers for the eight-partite linear CV cluster state consisting of the eight output modes $\hat{b}_j$ ($j = 1, \ldots, 8$), which are $\delta_{L1} = \sqrt{2}\mathrm{e}^{-r}\hat{x}_1^{(0)}$, $\delta_{L2} = \sqrt{3}\mathrm{e}^{-r}\hat{p}_2^{(0)}$, $\delta_{L3} = \frac{1}{\sqrt{2}}\mathrm{e}^{-r}\hat{x}_1^{(0)} - \sqrt{\frac{5}{2}}\mathrm{e}^{-r}\hat{x}_3^{(0)}$, $\delta_{L4} = \frac{1}{\sqrt{3}}\mathrm{e}^{-r}\hat{p}_2^{(0)} + \sqrt{\frac{2}{5}}\mathrm{e}^{-r}\hat{p}_6^{(0)} + \sqrt{\frac{34}{15}}\mathrm{e}^{-r}\hat{x}_5^{(0)}$, $\delta_{L5} = \sqrt{\frac{34}{15}}\mathrm{e}^{-r}\hat{p}_4^{(0)} - \sqrt{\frac{2}{5}}\mathrm{e}^{-r}\hat{x}_3^{(0)} - \frac{1}{\sqrt{3}}\mathrm{e}^{-r}\hat{x}_7^{(0)}$, $\delta_{L6} = \sqrt{\frac{5}{2}}\mathrm{e}^{-r}\hat{p}_6^{(0)} - \frac{1}{\sqrt{2}}\mathrm{e}^{-r}\hat{p}_8^{(0)}$, $\delta_{L7} = -\sqrt{3}\mathrm{e}^{-r}\hat{x}_7^{(0)}$ and $\delta_{L8} = -\sqrt{2}\mathrm{e}^{-r}\hat{p}_8^{(0)}$, respectively.

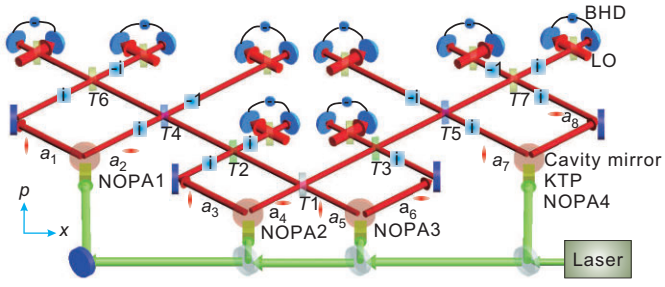

Figure 2 (Color online) Schematic of experimental setup for CV eight-partite cluster state generation. T: transmission efficient of beam splitter, Boxes including i are Fourier transforms (90° rotations in phase space), −i is a −90° rotation, and −1 is a 180° rotation, BHD: balanced homodyne detector.

The unitary matrix of the two-diamond cluster state U_D equals to $U_F U_L$, with $U_F = \mathrm{diag}\{-1, -\mathrm{i}, \mathrm{i}, 1, 1, \mathrm{i}, -\mathrm{i}, -1\}$, thus the two-diamond shape cluster state can be prepared from the linear cluster state via local Fourier transforms and phase rotations. The excess noise terms of the nullifiers of the two-diamond shape cluster state are expressed by $\delta_{D1} = -\frac{1}{\sqrt{2}}\mathrm{e}^{-r}\hat{x}_1^{(0)} + \sqrt{\frac{5}{2}}\mathrm{e}^{-r}\hat{x}_3^{(0)}$, $\delta_{D2} = \frac{1}{\sqrt{2}}\mathrm{e}^{-r}\hat{x}_1^{(0)} - \sqrt{\frac{5}{2}}\mathrm{e}^{-r}\hat{x}_3^{(0)}$, $\delta_{D3} = -\sqrt{3}\mathrm{e}^{-r}\hat{p}_2^{(0)}$, $\delta_{D4} = -\frac{2}{\sqrt{3}}\mathrm{e}^{-r}\hat{p}_2^{(0)} + \sqrt{\frac{2}{5}}\mathrm{e}^{-r}\hat{p}_6^{(0)} + \sqrt{\frac{34}{15}}\mathrm{e}^{-r}\hat{x}_5^{(0)}$, $\delta_{D5} = \sqrt{\frac{34}{15}}\mathrm{e}^{-r}\hat{p}_4^{(0)} - \sqrt{\frac{2}{5}}\mathrm{e}^{-r}\hat{x}_3^{(0)} + \frac{2}{\sqrt{3}}\mathrm{e}^{-r}\hat{x}_7^{(0)}$, $\delta_{D6} = \sqrt{3}\mathrm{e}^{-r}\hat{x}_7^{(0)}$, $\delta_{D7} = \sqrt{\frac{5}{2}}\mathrm{e}^{-r}\hat{p}_6^{(0)} - \frac{1}{\sqrt{2}}\mathrm{e}^{-r}\hat{p}_8^{(0)}$, and $\delta_{D8} = \sqrt{\frac{5}{2}}\mathrm{e}^{-r}\hat{p}_6^{(0)} + \frac{1}{\sqrt{2}}\mathrm{e}^{-r}\hat{p}_8^{(0)}$, respectively. According to the inseparability criteria for CV multipartite entangled states proposed by van Loock and Furusawa [39], we can deduce the inseparability criterion inequalities for CV eight-partite linear and two-diamond shape cluster states, which are given by eqs. (3a)–(3g) and eqs. (4a)–(4i), respectively.

$$V(\hat{p}_{L1} - \hat{x}_{L2}) + V(\hat{p}_{L2} - \hat{x}_{L1} - g_{L3}\hat{x}_{L3}) < 1, \quad (3a)$$
$$V(\hat{p}_{L2} - g_{L1}\hat{x}_{L1} - \hat{x}_{L3}) + V(\hat{p}_{L3} - \hat{x}_{L2} - g_{L4}\hat{x}_{L4}) < 1, \quad (3b)$$
$$V(\hat{p}_{L3} - g_{L2}\hat{x}_{L2} - \hat{x}_{L4}) + V(\hat{p}_{L4} - \hat{x}_{L3} - g_{L5}\hat{x}_{L5}) < 1, \quad (3c)$$
$$V(\hat{p}_{L4} - g_{L3}\hat{x}_{L3} - \hat{x}_{L5}) + V(\hat{p}_{L5} - \hat{x}_{L4} - g_{L6}\hat{x}_{L6}) < 1, \quad (3d)$$
$$V(\hat{p}_{L5} - g_{L4}\hat{x}_{L4} - \hat{x}_{L6}) + V(\hat{p}_{L6} - \hat{x}_{L5} - g_{L7}\hat{x}_{L7}) < 1, \quad (3e)$$
$$V(\hat{p}_{L6} - g_{L5}\hat{x}_{L5} - \hat{x}_{L7}) + V(\hat{p}_{L7} - \hat{x}_{L6} - g_{L8}\hat{x}_{L8}) < 1, \quad (3f)$$
$$V(\hat{p}_{L7} - g_{L6}\hat{x}_{L6} - \hat{x}_{L8}) + V(\hat{p}_{L8} - \hat{x}_{L7}) < 1, \quad (3g)$$

and

$$V(\hat{p}_{D1} - \hat{x}_{D3} - g_{D1}\hat{x}_{D4}) + V(\hat{p}_{D3} - \hat{x}_{D1} - g_{D2}\hat{x}_{D2}) < 1, \quad (4a)$$
$$V(\hat{p}_{D2} - \hat{x}_{D3} - g_{D1}\hat{x}_{D4}) + V(\hat{p}_{D3} - \hat{x}_{D2} - g_{D2}\hat{x}_{D1}) < 1, \quad (4b)$$
$$V(\hat{p}_{D1} - g_{D3}\hat{x}_{D3} - \hat{x}_{D4}) + V(\hat{p}_{D4} - \hat{x}_{D1} - g_{D4}\hat{x}_{D2} - g_{D5}\hat{x}_{D5}) < 1, \quad (4c)$$
$$V(\hat{p}_{D2} - g_{D3}\hat{x}_{D3} - \hat{x}_{D4}) + V(\hat{p}_{D4} - g_{D4}\hat{x}_1 - \hat{x}_{D2} - g_{D5}\hat{x}_{D5}) < 1, \quad (4d)$$
$$V(\hat{p}_{D4} - g_{D6}\hat{x}_{D1} - g_{D6}\hat{x}_{D2} - \hat{x}_{D5}) + V(\hat{p}_{D5} - \hat{x}_{D4} - g_{D6}\hat{x}_{D7} - g_{D6}\hat{x}_{D8}) < 1, \quad (4e)$$
$$V(\hat{p}_{D5} - g_{D5}\hat{x}_{D4} - \hat{x}_{D7} - g_{D4}\hat{x}_{D8}) + V(\hat{p}_{D7} - \hat{x}_{D5} - g_{D3}\hat{x}_{D6}) < 1, \quad (4f)$$
$$V(\hat{p}_{D5} - g_{D5}\hat{x}_{D4} - g_{D4}\hat{x}_{D7} - \hat{x}_{D8}) + V(\hat{p}_{D8} - \hat{x}_{D5} - g_{D3}\hat{x}_{D6}) < 1, \quad (4g)$$
$$V(\hat{p}_{D6} - \hat{x}_{D7} - g_{D2}\hat{x}_{D8}) + V(\hat{p}_{D7} - g_{D1}\hat{x}_{D5} - \hat{x}_{D6}) < 1, \quad (4h)$$
$$V(\hat{p}_{D6} - g_{D2}\hat{x}_{D7} - \hat{x}_{D8}) + V(\hat{p}_{D8} - g_{D1}\hat{x}_{D5} - \hat{x}_{D6}) < 1, \quad (4i)$$

where left-hand sides and right-hand sides of these inequalities are the combination of variances of nullifiers and the boundary, respectively.

The experimentally measured initial squeezing degrees of the output fields from four NOPAs are (4.30 ± 0.07) dB below the QNL which corresponds to the squeezing parameter $r = 0.50 \pm 0.02$. During the measurements the pump power of NOPAs at 540 nm wavelength is ~ 180 mW, which is below the oscillation threshold of 240 mW, and the intensity of the injected signal at 1080 nm is 10 mW. The phase difference on each beam-splitters are locked according to the requirements. The light intensity of the local oscillator in all BHDs is set to approximately 5 mW. The measured QNL is approximately 20 dB above the electronics noise level, which guarantees that the results of the homodyne detections are almost not affected by electronic noises.

The correlation variances measured experimentally are shown in Figure 3 for the linear cluster and Figure 4 for the two-diamond cluster. They are $V(\hat{p}_{L1} - \hat{x}_{L2}) = (-2.67 \pm 0.06)$ dB, $V(\hat{p}_{L2} - \hat{x}_{L1} - \hat{x}_{L3}) = (-2.65 \pm 0.13)$ dB, $V(\hat{p}_{L3} - \hat{x}_{L2} - \hat{x}_{L4}) = (-2.52 \pm 0.20)$ dB, $V(\hat{p}_{L4} - \hat{x}_{L3} - \hat{x}_{L5}) = (-2.69 \pm 0.09)$ dB, $V(\hat{p}_{L5} - \hat{x}_{L4} - \hat{x}_{L6}) = (-2.68 \pm 0.08)$ dB, $V(\hat{p}_{L6} - \hat{x}_{L5} - \hat{x}_{L7}) = (-2.56 \pm 0.10)$ dB, $V(\hat{p}_{L7} - \hat{x}_{L6} - \hat{x}_{L8}) = (-2.22 \pm 0.09)$ dB, $V(\hat{p}_{L8} - \hat{x}_{L7}) = (-2.21 \pm 0.09)$ dB and $V(\hat{p}_{D1} - \hat{x}_{D3} - \hat{x}_{D4}) = (-2.61 \pm 0.10)$ dB, $V(\hat{p}_{D2} - \hat{x}_{D3} - \hat{x}_{D4}) = (-2.57 \pm 0.09)$ dB, $V(\hat{p}_{D3} - \hat{x}_{D1} - \hat{x}_{D2}) = (-2.39 \pm 0.06)$ dB, $V(\hat{p}_{D4} - \hat{x}_{D1} - \hat{x}_{D2} - \hat{x}_{D5}) = (-2.58 \pm 0.09)$ dB, $V(\hat{p}_{D5} - \hat{x}_{D4} - \hat{x}_{D7} - \hat{x}_{D8}) = (-2.61 \pm 0.09)$ dB, $V(\hat{p}_{D6} - \hat{x}_{D7} - \hat{x}_{D8}) = (-2.52 \pm 0.10)$ dB, $V(\hat{p}_{D7} - \hat{x}_{D5} - \hat{x}_{D6}) = (-2.59 \pm 0.09)$ dB, $V(\hat{p}_{D8} - \hat{x}_{D5} - \hat{x}_{D6}) = (-2.58 \pm 0.10)$ dB, $V(\hat{p}_{D4} - g_{D6}\hat{x}_{D1} - g_{D6}\hat{x}_{D2} - \hat{x}_{D5}) = (-1.57 \pm 0.09)$ dB, $V(\hat{p}_{D5} - \hat{x}_{D4} - g_{D6}\hat{x}_{D7} - g_{D6}\hat{x}_{D8}) = (-1.53 \pm 0.09)$ dB. From these measured results we can calculate the combinations of the correlation variances in the left-hand sides of the inequalities (3a)–(3g) and (4a)–(4i), which are 0.68 ± 0.02, 0.83 ± 0.02, 0.82 ± 0.02, 0.81 ± 0.02, 0.82 ± 0.02, 0.87 ± 0.02, 0.75 ± 0.02, for the linear cluster and 0.84 ± 0.02, 0.85 ± 0.02, 0.96 ± 0.02, 0.97 ± 0.02, 0.95 ± 0.02, 0.96 ± 0.02, 0.96 ± 0.02, 0.83 ± 0.02, 0.83 ± 0.02 for the two-diamond cluster, respectively. All these values are smaller than the normalized boundary. This indicates that the prepared two types of CV cluster states satisfy the inseparability criteria for verifying multipartite CV entanglement, so the spatially separated eight-partite entangled states of qumodes are experimentally obtained. In the experiment we detected the correlation variances under $g_{L1-L8} = 1$, $g_{D1-D5} = 1$ and $g_{D6} = g_{D6}^{\mathrm{opt}} = 0.60 \pm 0.02$ (g^{opt} is the optimal gain factor). For our system, the total transmission efficiency of squeezed beams are about 87% and the detection efficiency is about 90%, which leads to the efficient squeezing parameter as being $r_e = 0.30$ which is smaller than the initially measured squeezing parameter. When the gain factors except g_{D6} are taken as 1 and only g_{D6}^{opt} is utilized, all inequalities in eqs. (3) and (4) are satisfied.

2 The research progress on the generation of multi-color entanglement

2.1 Two-color entanglement

Non-degenerate optical parametric oscillators (NOPOs) above the oscillation threshold are the most successful devices for the experimental generation of the multi-color CV

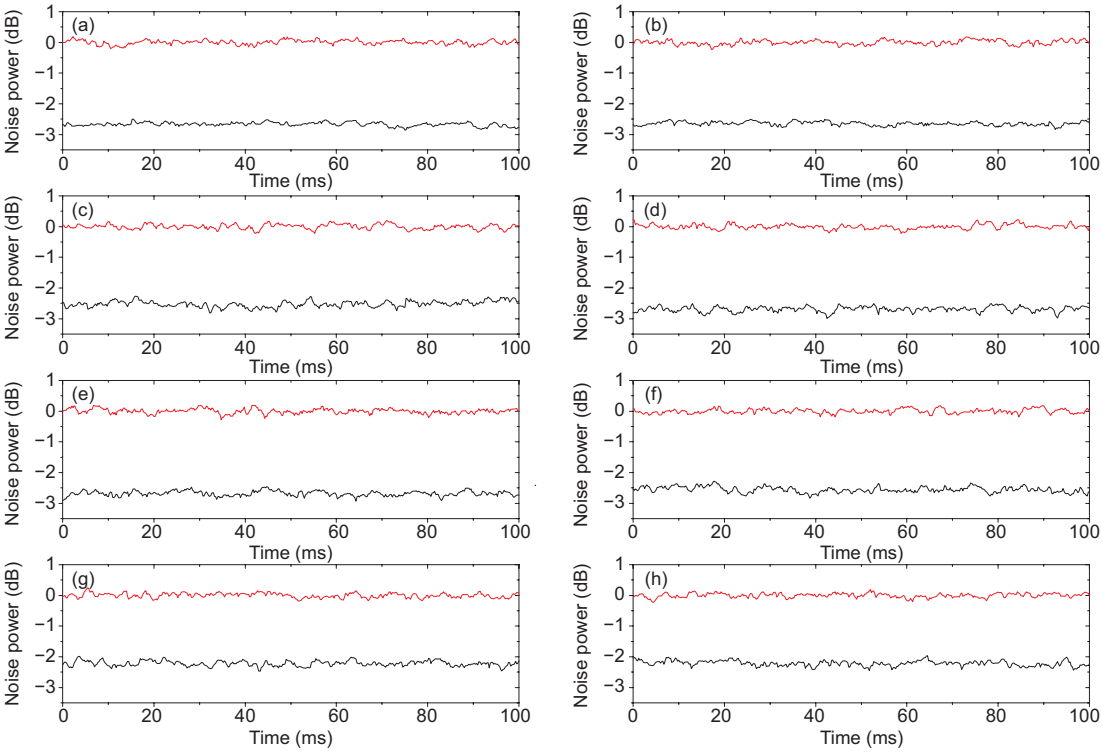

Figure 3 (Color online) Measured noise powers of eight-partite linear cluster state. The upper and lower lines in all graphs are shot noise level and correlation variances of nullifiers, respectively. (a)–(h) are noise powers of $V(\hat{p}_{L1} - \hat{x}_{L2})$, $V(\hat{p}_{L2} - \hat{x}_{L1} - \hat{x}_{L3})$, $V(\hat{p}_{L3} - \hat{x}_{L2} - \hat{x}_{L4})$, $V(\hat{p}_{L4} - \hat{x}_{L3} - \hat{x}_{L5})$, $V(\hat{p}_{L5} - \hat{x}_{L4} - \hat{x}_{L6})$, $V(\hat{p}_{L6} - \hat{x}_{L5} - \hat{x}_{L7})$, $V(\hat{p}_{L7} - \hat{x}_{L6} - \hat{x}_{L8})$, and $V(\hat{p}_{L8} - \hat{x}_{L7})$, respectively. The measurement frequency is 2 MHz, resolution bandwidth is 30 kHz, and video bandwidth is 100 Hz [23].

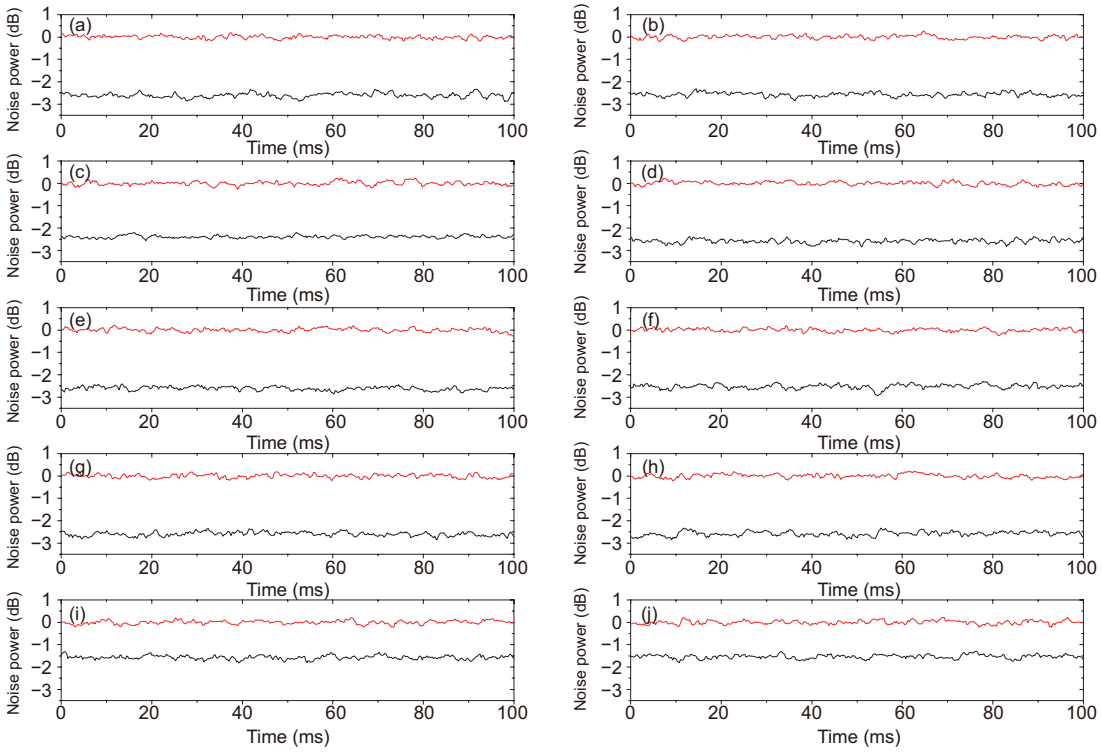

Figure 4 (Color online) Measured noise powers of eight-partite two-diamond shape cluster state. The upper and lower lines in all graphs are shot noise level and correlation variances of nullifiers, respectively. (a)–(j) are noise powers of $V(\hat{p}_{D1} - \hat{x}_{D3} - \hat{x}_{D4})$, $V(\hat{p}_{D2} - \hat{x}_{D3} - \hat{x}_{D4})$, $V(\hat{p}_{D3} - \hat{x}_{D1} - \hat{x}_{D2})$, $V(\hat{p}_{D4} - \hat{x}_{D1} - \hat{x}_{D2} - \hat{x}_{D5})$, $V(\hat{p}_{D5} - \hat{x}_{D4} - \hat{x}_{D7} - \hat{x}_{D8})$, $V(\hat{p}_{D6} - \hat{x}_{D7} - \hat{x}_{D8})$, $V(\hat{p}_{D7} - \hat{x}_{D5} - \hat{x}_{D6})$, $V(\hat{p}_{D8} - \hat{x}_{D5} - \hat{x}_{D6})$, $V(\hat{p}_{D4} - g_{D6}\hat{x}_{D1} - g_{D6}\hat{x}_{D2} - \hat{x}_{D5})$, $V(\hat{p}_{D5} - \hat{x}_{D4} - g_{D6}\hat{x}_{D7} - g_{D6}\hat{x}_{D8})$, respectively. The measurement frequency is 2 MHz, resolution bandwidth is 30 kHz, and video bandwidth is 100 Hz [24].

entangled optical beams [40–46]. Two-color entangled optical beams at different frequency regions have been experimentally prepared by means of above-threshold NOPOs with various pump lasers and nonlinear crystals [40–44]. The first measurement of squeezed-state entanglement of the twin beams between bright fields of truly different frequencies produced in a NOPO operating above threshold was reported by Villar et al. [40]. They used a 532 nm laser to pump a NOPO and record noise spectra of the generated beams with the synchronous analysis cavity, the squeezing in the intensity difference as well as the sum of phase between the twin beams were measured simultaneously [40]. Successively, the quantum entanglement of amplitude (−1.25 dB) and phase quadratures (−0.60 dB) between two intense optical beams with a total intensity of 22 mW and a frequency difference of 1 nm has been experimentally verified by the authors, in which the quantum correlation noise was measured by two sets of unbalanced Mach-Zehnder interferometers [41]. Jing et al. [42] observed CV entanglement between the bright beams emitted above threshold by an ultra-stable NOPO, classically phase locked at a frequency difference of 161.827324 MHz. The measured amplitude-difference squeezing and the phase-sum squeezing are −3 dB and −1.35 dB, respectively [42]. Recently, bright two-color CV entangled optical beams at 800 nm and 1500 nm has been experimentally generated by Li et al. [44]. In the experiment, a phase-insensitive optical parametric amplifier with a single injection beam at 1500 nm was utilized. Without locking the relative phase between the signal and pump fields, the amplitude quadrature difference squeezing of −3.30 dB and phase quadrature sum squeezing of −3.35 dB were observed, which satisfy the entanglement criterion [44].

2.2 Three-color entanglement

During past years, to satisfy the requirements of the developing QI networks the generation schemes of multi-color CV entangled states via intra-cavity nonlinear processes have been theoretically proposed [47–49]. In 2009, the first CV three-color entangled state was experimentally produced by an above-threshold NOPO at a low temperature of −23°C [45]. The three entangled sub-modes produced in this experiment are the output signal, idler and reflected pump modes from a NOPO above the threshold, the wavelengths are 1062.102 nm, 1066.915 nm and 532.251 nm, respectively. For developing practical CV QI networks with both nodes and fiber transmission lines, it is important to prepare multi-partite entangled states consisting of optical sub-modes at variously designated wavelengths.

For reducing the influence of the phonon noise on the reflected pump field and improving the wavelength selectivity of the system, we proposed a generation system of CV three-color entangled optical beams, in which two cascaded NOPO1 and NOPO2 are utilized [46,49]. The idler optical beams produced by NOPO1, is used for the pump light of NOPO2. The three-color entanglement among signal and idler beams produced by NOPO2 and the retained signal beam from NOPO1 is theoretically demonstrated and the optimal operation conditions of the cascaded NOPOs system are numerically analyzed in ref. [49]. Following the theoretical design we have achieved the experimental generation of three-color CV entangled state by using the cascaded NOPOs system for the first time [46]. Through the special selections of the pump laser and the nonlinear crystals in the two NOPOs, the wavelength of one of the obtained three-color entangled beams is 852 nm which can be tuned to a transition frequency of Cs atoms thus can be used for the storage of quantum information. The wavelengths of other two beams are 1550 nm matched for optimal transmission in optical fibers and 1440 nm close to the fiber window with comparatively low transmission losses. The produced three-color CV entangled states are suitable to be applied in the future quantum information networks containing both atomic storage unit and optical fiber transmission line.

Figure 5 shows the principle schematic of the three-color entanglement generation system, which consists of NOPO1 and NOPO2. The coherent optical field at 795 nm from a continuous-wave Ti: Sapphire laser (MBR110, Coherent Ltd.) is frequency-doubled by a second harmonic generator (SHG) to obtain the light at 398 nm (a_0) for pumping the NOPO1 to create a pair of intense optical beams (a_1 and a_2), The generated idler beam (a_1^{out}) drives the NOPO2 to achieve the cascaded intra-cavity optical parametric down-conversion and to produce the output fields a_3 and a_4. Both NOPO1 and NOPO2 are in a Fabre-Perot cavity configuration consisting of two concave mirrors with a 50-mm radius curvature. For obtaining the desired frequencies two different nonlinear crystals are chosen respectively for the two NOPOs, which are 1 mm × 2 mm × 10 mm^3 PPKTP for NOPO1 and 1 mm×2 mm×10 mm^3 PPLN (periodically poled lithium niobate) for NOPO2. The temperature of two nonlinear crystals are controlled by an electronic temperature-controller with the precision of 0.01°C (YG-IIS-RA, Yuguang Ltd.). It has been theoretically shown by Tan et al. [49] that the three final output light beams (a_2, a_3 and a_4) have strong intensity correlation. On the other hand, the frequency constraint among the three optical modes translates into a constraint for the phase variations, so the phase fluctuations of the optical modes a_1 and a_2 (a_3 and a_4) should be anti-correlated each other, the sum of their phase fluctuations should be correlated with the phase fluctuation of the pump field. Three M-Z interferometers with unbalanced arm lengths are applied to measure the noise powers of the phase and the amplitude quadratures for the three resultant subharmonic modes of a_2, a_3 and a_4 as well as to determine the corresponding QNLs [41,50]. The noise powers measured simultaneously by the three M-Z interferometers are combined by the positive or negative power combiners and then the combined correlations variances of the amplitude and the phase quadratures are analyzed by a spectrum analyzer.

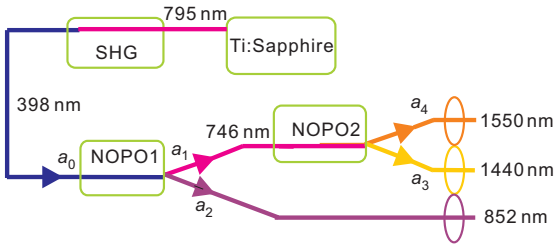

Figure 5 (Color online) Principle schematic of the three-color entanglement generation system.

The measured correlation variances of the noise powers of the amplitude and the phase quadratures among the three resultant optical beams at 852.35 nm, 1550.60 nm and 1440.06 nm are shown in Figures 6(a)–(f), where the traces (i) and the traces (ii) stand for the QNLs and the correlation variances, respectively. From Figure 6 we have $\langle\delta^2(X_3 - X_4)\rangle = (-4.1 \pm 0.1)$ dB, $\langle\delta^2(g_1^{\rm opt}Y_2 + Y_3 + Y_4)\rangle = (-1.1 \pm 0.1)$ dB, $\langle\delta^2(X_2 - X_3)\rangle = (-3.2 \pm 0.1)$ dB, $\langle\delta^2(Y_2 + g_2^{\rm opt}Y_3 + Y_4)\rangle = (-0.5 \pm 0.1)$ dB, $\langle\delta^2(X_2 - X_4)\rangle = (-3.2 \pm 0.1)$ dB and $\langle\delta^2(Y_2 + Y_3 + g_3^{\rm opt}Y_4)\rangle = (-0.5 \pm 0.1)$ dB. The minus symbol before the first numbers in the right sides of these equalities indicates that the variances are below the corresponding QNL and $g_j^{\rm opt}$ ($j = 1, 2, 3$) represents the optimal gain values of g_j taken in the experiment for obtaining the highest correlations [39]. The three combinations of the correlation variances are

$$\begin{aligned}
&\langle\delta^2(X_3 - X_4)\rangle + \langle\delta^2(g_1^{\rm opt}Y_2 + Y_3 + Y_4)\rangle = 0.76 < 1,\\
&\langle\delta^2(X_2 - X_4)\rangle + \langle\delta^2(Y_2 + g_2^{\rm opt}Y_3 + Y_4)\rangle = 0.92 < 1,\\
&\langle\delta^2(X_2 - X_3)\rangle + \langle\delta^2(Y_2 + Y_3 + g_3^{\rm opt}Y_4)\rangle = 0.92 < 1.
\end{aligned} \quad (5)$$

All of them are smaller than the criteria "1" for the CV three-partite entanglement of optical modes. Thus, the three-color CV entanglement is experimentally demonstrated.

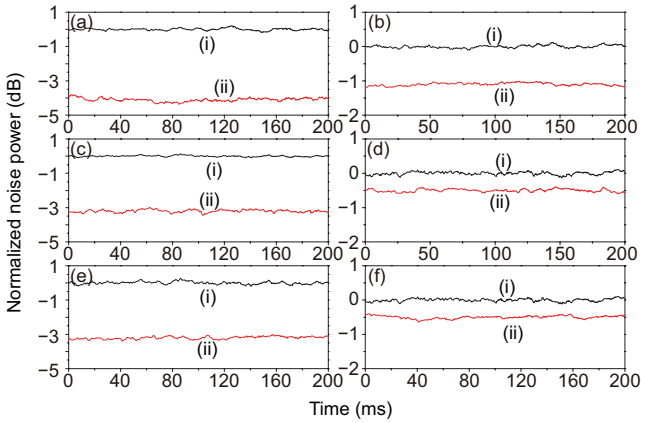

Figure 6 (Color online) The measured correlation variance of three-color entangled states at 2 MHz. (a) $\langle\delta^2(X_3 - X_4)\rangle$; (b) $\langle\delta^2(g_1^{\rm opt}Y_2 + Y_3 + Y_4)\rangle$; (c) $\langle\delta^2(X_2 - X_4)\rangle$; (d) $\langle\delta^2(Y_2 + g_2^{\rm opt}Y_3 + Y_4)\rangle$; (e) $\langle\delta^2(X_2 - X_3)\rangle$; (f) $\langle\delta^2(Y_2 + Y_3 + g_3^{\rm opt}Y_4)\rangle$. (i) The QNL; (ii) The correlation noise power. The measurement parameters of SA: RBW 30 kHz; VBW 100 Hz [46].

3 Conclusion

We have reviewed the experimental progress in the preparations of cluster states and multi-color entangled states. The multipartite entangled states are the essential resources to construct a variety of CVQI networks. The complexity and versatility of CV multipartite entanglement for qumodes not only offer richly potential applications in QC and QI, but also provide the basic and handleable entangled quantum states which can be an important tool for further studying and understanding quantum entanglement phenomena as well as the unusual conventions of quantum mechanics.

This work was supported by the National Basic Research Program of China (Grant No. 2010CB923103) and the National Natural Science Foundation of China (Grant Nos. 11322440, 11074157, 11174188 and 61121064) and OIT and Shanxi Scholarship Council of China (Grant No. 2012-010).

1 Nielsen M A, Chuang I L. Quantum Computation and Quantum Information. Cambridge: Cambridge University Press, 2000
2 Braunstein S L, Pati A K. Quantum Information with Continuous Variables. Berlin: Springer, 2003
3 Bouwmeester D, Ekert A, Zeilinger A. The Physics of Quantum Information. Berlin: Springer, 2000
4 Bouwmeester D, Pan J W, Mattle K, et al. Experimental quantum teleportation. Nature, 1997, 390: 575–579
5 Furusawa A, Sorensen J L, Braustein S L, et al. Unconditional quantum teleportation. Science, 1998, 282: 706–709
6 Mattle K, Weinfurter H, Kwiat P G, et al. Dense coding in experimental quantum communication. Phys Rev Lett, 1996, 76: 4656–4659
7 Li X Y, Pan Q, Jing J T, et al. Quantum dense coding exploiting a bright Einstein-Podolsky-Rosen beam. Phys Rev Lett, 2002, 88: 047904
8 Walther P, Resch K J, Rudolphet T, et al. Experimental one-way quantum computing. Nature, 2005, 434: 169–176
9 Chen K, Li C M, Zhang Q, et al. Experimental realization of one-way quantum computing with two-photon four-qubit cluster states. Phys Rev Lett, 2007, 99: 120503
10 Wang Y, Su X L, Shen H, et al. Toward demonstrating controlled-X operation based on continuous-variable four-partite cluster states and quantum teleporters. Phys Rev A, 2010, 81: 022311
11 Ukai R, Yokoyama S, Yoshikawa J I, et al. Demonstration of a controlled-phase gate for continuous-variable one-way quantum computation. Phys Rev Lett, 2011, 107: 250501
12 Raussendorf R, Briegel H J. A one-way quantum computer. Phys Rev Lett, 2001, 86: 5188–5191
13 Menicucci N C, van Loock P, Gu M, et al. Universal quantum computation with continuous-variable cluster states. Phys Rev Lett, 2006, 97: 110501
14 Zhang J, Braunstein S L. Continuous-variable Gaussian analog of cluster states. Phys Rev A, 2006, 73: 032318
15 Van Loock P, Weedbrook C, Gu M. Building Gaussian cluster states by linear optics. Phys Rev A, 2007, 76: 032321
16 Gu M, Weedbrook C, Menicucci N C, et al. Quantum computing with continuous-variable clusters. Phys Rev A, 2009, 79: 062318
17 Van Loock P. Examples of Gaussian cluster computation. J Opt Soc Am B, 2007, 24: 340–346

18 Tan A H, Xie C D, Peng K C. Quantum logical gates with linear quadripartite cluster states of continuous variables. Phys Rev A, 2009, 79: 042338

19 Miwa Y, Yoshikawa J I, van Loock P, et al. Demonstration of a universal one-way quantum quadratic phase gate. Phys Rev A, 2009, 80: 050303(R)

20 Ukai R, Iwata N, Shimokawa Y, et al. Demonstration of unconditional one-way quantum computations for continuous variables. Phys Rev Lett, 2011, 106: 240504

21 Huang Y F, Liu B H, Peng L, et al. Experimental generation of an eight-photon Greenberger-Horne-Zeilinger state. Nat Commun, 2011, 2: 546

22 Yao X C, Wang T X, Xu P, et al. Observation of eight-photon entanglement. Nat Photon, 2012, 6: 225–228

23 Su X L, Zhao Y P, Hao S H, et al. Experimental preparation of eight-partite cluster state for photonic qumodes. Opt Lett, 2012, 37: 5178–5180

24 Su X L, Hao S H, Zhao Y P, et al. Demonstration of eight-partite two-diamond shape cluster state for continuous variables. Front Phys, 2013, 8: 20–26

25 Yokoyama S, Ukai R, Armstrong S C, et al. Optical generation of ultra-large-scale continous-variable cluster states. arxiv:1306.3366v1

26 Kimble H J. The quantum internet. Nature, 2008, 453: 1023–1030

27 Jia X J, Zhang J, Wang Y, et al. Superactivation of multipartite unlockable bound entanglement. Phys Rev Lett, 2012, 108: 190501

28 Jing J, Zhang J, Yan Y, et al. Experimental demonstration of tripartite entanglement and controlled dense coding for continuous variables. Phys Rev Lett, 2003, 90: 167903

29 Yonezawa H, Aoki T, Furusawa A. Demonstration of a quantum teleportation network for continuous variables. Nature, 2004, 431: 430–433

30 Lance A M, Symul T, Bowen W P, et al. Tripartite quantum state sharing. Phys Rev Lett, 2004, 92: 177903

31 Su X L, Tan A, Jia X, et al. Experimental preparation of quadripartite cluster and Greenberger-Horne-Zeilinger entangled states for continuous variables. Phys Rev Lett, 2007, 98: 070502

32 Yukawa M, Ukai R, van Loock P, et al. Experimental generation of four-mode continuous-variable cluster states. Phys Rev A, 2008, 78: 012301

33 Tan A H, Wang Y, Jin X L, et al. Experimental generation of genuine four-partite entangled states with total three-party correlation for continuous variables. Phys Rev A, 2008, 78: 013828

34 Pysher M, Miwa Y, Shahrokhshahi R, et al. Parallel generation of quadripartite cluster entanglement in the optical frequency comb. Phys Rev Lett, 2011, 107: 030505

35 Armstrong S, Morizur J F, Janousek J, et al. Programmable multimode quantum networks. Nat Commun, 2012, 3: 1026

36 Wang Y J, Zheng Y H, Xie C D, et al. High-power low-noise Nd: YAP/LBO laser with dual wavelength outputs. IEEE J Quantum Electron, 2011, 47: 1006–1013

37 Wang Y, Shen H, Jin X L, et al. Experimental generation of 6 dB continuous variable entanglement from a nondegenerate optical parametric amplifier. Opt Express, 2010, 18: 6149–6155

38 Zhang Y, Wang H, Li X Y, et al. Experimental generation of bright two-mode quadrature squeezed light from a narrow-band nondegenerate optical parametric amplifier. Phys Rev A, 2000, 62: 023813

39 Van Loock P, Furusawa A. Detecting genuine multipartite continuous-variable entanglement. Phys Rev A, 2003, 67: 052315

40 Villar A S, Cruz L S, Cassemiro K N, et al. Generation of bright two-color continuous variable entanglement. Phys Rev Lett, 2005, 95: 243603

41 Su X L, Tan A H, Jia X J, et al. Experimental demonstration of quantum entanglement between frequency-nondegenerate optical twin beams. Opt Lett, 2006, 31: 1133–1135

42 Jing J, Feng S, Bloomer R, et al. Experimental continuous-variable entanglement from a phase-difference-locked optical parametric oscillator. Phys Rev A, 2006, 74: 041804

43 Keller G, D'Auria V, Treps N, et al. Experimental demonstration of frequency-degenerate bright EPR beams with a self-phase-locked OPO. Opt Express, 2008, 16: 9351–9356

44 Li Y M, Guo X M, Bai Z L, et al. Generation of two-color continuous variable quantum entanglement at 0.8 and 1.5 μm. App Phys Lett, 2010, 97: 031107

45 Coelho A S, Barbosa F A S, Cassemiro K N, et al. Three-color entanglement. Science, 2009, 326: 823–826

46 Jia X J, Yan Z H, Duan Z Y, et al. Experimental realization of three-color entanglement at optical fiber communication and atomic storage wavelengths. Phys Rev Lett, 2012, 109: 253604

47 Villar A S, Martinelli M, Fabre C, et al. Direct production of tripartite pump-signal-idler entanglement in the above-threshold optical parametric oscillator. Phys Rev Lett, 2006, 97: 140504

48 Cassemiro K N, Villar A S. Scalable continuous-variable entanglement of light beams produced by optical parametric oscillators. Phys Rev A, 2008, 77: 022311

49 Tan A H, Xie C D, Peng K C. Bright three-color entangled state produced by cascaded optical parametric oscillators. Phys Rev A, 2012, 85: 013819

50 Glockl O, Andersen U L, Lorenz S, et al. Sub-shot-noise phase quadrature measurement of intense light beams. Opt Lett, 2004, 29: 1936–1938